Material Properties of Nanocrystalline Silicon Carbide for Transparent Passivating Contact Solar Cells

Alexander Eberst,* Andreas Lambertz, Weiyuan Duan, Vladimir Smirnov, Uwe Rau, and Kaining Ding

Due to its high transparency, silicon carbide can replace amorphous silicon as a front contact material in crystalline silicon solar cells. Herein, first a look at doping in nc-SiC:H with different deposition techniques is taken. Then, the influence of various deposition conditions for hot wire chemical vapor deposition-prepared nc-SiC:H is investigated. Both the electrical conductivity and the optical bandgap increase simultaneously for a multitude of deposition parameters. Combining a high filament temperature of the catalytic filament, a high hydrogen dilution of the precursor gas and an overall low total gas flow, conductivities of 0.38 S cm^{-1} in combination with an optical bandgap of 3.2 eV can be achieved. In the last section, a closer look into the dependencies of the layer thicknesses of the two different nc-SiC:H layers applied in solar cells on the cell performance is taken. While the layer with conducting properties only has minor influences on cell properties, a trade-off between passivation and fill factor is identified for the passivating nc-SiC:H layer. For thicker layers, the passivating nc-SiC:H layer achieves a very high implied open-circuit voltage above 740 mV, but the fill factor starts to degrade due to a very low conductance of the layer.

1. Introduction

The current focus in research for a steady increase in efficiency of silicon solar cells is passivated contacts, where passivating, conductive, and transparent interlayers are inserted between the metal contact and the crystalline silicon absorber.[1,2] One prominent approach is the silicon heterojunction (SHJ) solar cell, where intrinsic and doped hydrogenated amorphous silicon (a-Si:H) acts as interlayers. Here, one limitation is light which is parasitically absorbed in the a-Si:H and does not contribute to the current generated by the solar cell. Additional parasitic absorption is also happening in the transparent conductive oxide (TCO), which is needed for lateral current transport.[3] One possibility to reduce these losses is to use a wide-bandgap material like silicon oxide or silicon carbide, or try a dopant-free approach, which omits the doped a-Si:H and the TCO.[1,4] For silicon carbide, many attempts have been made to integrate it into various types of solar cell structures,[5–9] but the best results were achieved using a low-temperature approach by a wet-chemically grown silicon oxide in combination with two different nanocrystalline silicon carbide layers, one passivating and one conducting layer. This so-called transparent passivating contact (TPC) approach resulted in efficiencies of 23.99%.[8] With these promising results, it is worthwhile to revisit the material properties needed for the hydrogenated nanocrystalline silicon carbide (nc-SiC:H) to achieve such high cell efficiencies. This work gives a state-of-the-art overview of the material properties of nc-SiC:H and discusses the implementation of nc-SiC:H materials in TPC solar cells, demonstrating how the two different nc-SiC:H functional layers can be combined in a stack to improve the performance of the solar cells.

A. Eberst, A. Lambertz, W. Duan, V. Smirnov, U. Rau, K. Ding
IEK-5 Photovoltaik
Forschungszentrum Jülich GmbH
52425 Jülich, Germany
E-mail: a.eberst@fz-juelich.de

A. Eberst, U. Rau
Faculty of Electrical Engineering and Information Technology
RWTH Aachen University
52062 Aachen, Germany

The ORCID identification number(s) for the author(s) of this article can be found under https://doi.org/10.1002/solr.202300013.

2. Doping in Nanocrystalline Silicon Carbide

The development of silicon carbide (SiC) layers as a functional layer in photovoltaic devices started with its application in thin-film solar cells.[10] From then on, due to a favorable combination of the optical and electrical properties,[11,12] the material attracted a significant attention in the field of solar cell devices,[5–8,13–15] either only using amorphous (a-) or nanocrystalline (nc-) SiC or in combination with amorphous silicon or silicon oxide. The material can be deposited either by PECVD,[13,16] hot-wire chemical vapor deposition (HWCVD),[13,17] or even sputtering.[18] The unintentionally doped material has a strong n-type character but can additionally be n-type doped by nitrogen, phosphorous, or oxygen, as well as p-type doped by aluminum or boron.[13,16,17,19]

As HWCVD-prepared nc-SiC:H has the most promising optoelectrical properties and is well established in photovoltaic applications already, this work has a focus on the properties of HWCVD-grown nc-SiC:H but an additional comparison to PECVD-deposited materials will be given. Overall, the optoelectrical properties of the material are strongly influenced by the crystallite size of the material, which can be adjusted by the deposition conditions.[13,17] An explanation for the better performance in terms of transparency and conductivity of HWCVD-grown films compared to PECVD-grown films could be that the grain size of the crystallites is much larger when HWCVD is used, leading to an increased conductivity and transparency. One possible explanation is that in the HWCVD process, more low-energy hydrogen radicals are present, and less ion bombardment is happening. Hydrogen radicals are necessary for a higher crystallinity as they etch weakly bonded silicon atoms, leaving only the stronger crystalline bonds. An increased hydrogen radical density during the HWCVD deposition can be achieved by a higher hydrogen dilution, an increased filament temperature, and increased deposition pressure. Another important parameter is the residual time of the monomethylsilane (MMS) molecules in the chamber, giving the atoms more time to migrate to a favorable bonding site and forming a stronger bond. Overall, a lower deposition rate seems favorable for a larger crystallite size, since the molecules on the sample have more time to arrange themselves and weak bonds get etched away.[13,20] The process details during the layer growth will be discussed in depth later on.

The polytype of the crystalline SiC is, if reported, always 3C-SiC or the material is amorphous. No mixed polytype was detected.[21] Only for boron doping, crystallites in an amorphous silicon matrix are detected.[22] In HWCVD, an amorphous SiC phase was the result of very low filament temperatures (T_f) or a low hydrogen dilution gas concentration (c_H).[17] The grain size on the other hand is increased by high T_f, high c_H, a reduced total flow rate (F_{total}), or decreased filament–substrate distance (d_{f-s}).[13,17]

In the unintentionally doped material, a still rather high oxygen and nitrogen concentration can be found, both in the order of 10^{19} at cm^{-3}. Even for a fixed impurity concentration at this value, a variation in deposition conditions can result in a wide range of conductivities σ between 10^{-13} and 10^{+1} S cm^{-1}.[13] For PECVD-deposited nc-SiC:H, the conductivities typically lie in the range of 10^{-11}–10^{-3} S cm^{-1}.[13,17] For sputtered nc-SiC:H, the conductivities can be tuned from 10^{-11} to 10^{-5} S cm^{-1}, depending on the substrate temperature.[18] Also, for these deposition techniques, the increase in conductivity can be related to an increase in grain size. It is assumed that, similar to polycrystalline silicon,[23] the conductivity inside the grains is higher than in the grain boundary region due to imperfect bonding at the boundaries, leading to defect states which trap electrons, and produce a depletion region. The optical bandgap E_{04} is found to increase with increasing conductivity for the HWCVD-prepared film, as both are related to the crystallite size, while it slightly decreases for the PECVD-prepared films. For all samples, the sub-bandgap absorption from free charge carriers at α of 1 eV, α_{1eV}, in contrast also increases with increasing conductivity, and, thus, increasing crystallite size.[13]

Figure 3 shows that, in general, the PECVD-deposited material has a lower E_{04} and slightly lower conductivity as compared to the HWCVD-deposited material. Also, for the PECVD-deposited material, no strong difference in the optoelectronic parameters is found for the different doping sources. For the HWCVD-deposited material, the n-type-doped material, independent of the dopant, could achieve a higher optical bandgap than the p-type material. The highest E_{04} in combination with the highest σ could be achieved for nitrogen-doped HWCVD-deposited material.

For p-type doping, the naturally n-type character needs to be overdoped. Boron-doping strongly enhances the amorphous phase in PECVD-depositions, so that the doping gas concentrations need to be sufficient low to keep a nanocrystalline character of the material. This leads to conductivities in the order of 10^{-3} S cm^{-1}.[16] Similar conductivities are achieved by boron-doping using HWCVD, where the conductivity first increases, but starts to decrease again for high doping concentrations.[22] Using Al-doping, conductivities above 0.1 S cm^{-1} could be achieved.[19] Some results, in combination with results achieved in this work, are summarized in Figure 3.

For the controlled incorporation of oxygen and nitrogen, nitrogen seems to be the more suitable partner to increase the conductivity. It was shown that for oxygen incorporation, no strong increase in conductivity can be achieved before forming oxycarbide alloys and dramatically reducing the conductivity.[13] For nitrogen incorporation, the electrical conductivity could be tuned over five orders of magnitude. It is also found that the incorporation of impurities hinders the grain growth, and the grain size decreases for an increasing doping concentration.[13,17,22] Combining high nitrogen doping, a rather low F_{MMS} and a reduced d_{f-s} a conductivity of $\sigma = 14$ S cm^{-1} could be achieved by Pomaska.[13] For high doping concentrations, it was not possible to extract an E_{04} because α was always above 10^4 cm^{-1}.[13] With phosphorous incorporation, conductivities up to 5×10^{-2} S cm^{-1} (deposited by PECVD)[16] and 4.47×10^0 S cm^{-1} (deposited by HWCVD)[17] could be achieved. Overall, nitrogen doping seems favorable as n-type dopant as oxygen easily forms oxycarbides[13] and phosphorous has a lower doping efficiency.[17]

With the focus on T_f and solar cell application, more thorough investigations were performed on the nitrogen-doped case. It is confirmed that the conductivity increases strongly with T_f up to 0.1 S cm^{-1} for T_f up to 1,900 °C, after which the conductivity saturates for an increased T_f. It is found that the nitrogen concentration increases as well, while the oxygen concentration stays constant for increasing filament temperatures. For T_f above 1,900 °C, nearly all dopants are active, while the dopant activation exponentially decreases with decreasing T_f. It is assumed that for lower T_f, and, thus, lower crystallite size, the nitrogen cannot be incorporated in the grains and accumulate at the grain boundaries.[13] The previous results regarding the optical bandgap and sub-bandgap absorption are confirmed as well,[24] as it was shown that the E_{04} and α_{1eV} increase for increasing T_f. It is worth to mention that the increase in E_{04} seems to saturate for high T_f, while α_{1eV} increases exponentially, leading to a calculated parasitic absorption minimum for intermediate ($\approx$1800 °C) T_f.[24,25] The increase in E_{04} is attributed to the increased crystallite size as well. As α_{1eV} correlates with σ, but not with the crystallite size, it is attributed to free carrier absorption.[24]

The passivation capability of nc-SiC:H is investigated in solar cells, with a special focus again on T_f. Contrary to σ, the passivation, in terms of implied open-circuit voltage iV_{OC} and saturation current density J_0, decreases with increasing T_f, which is attributed to a lower hydrogen content of the material. The additional hydrogen supplied by the nc-SiC:H is necessary to satisfy the dangling bonds at the crystalline silicon interface, which, in the TPC approach, could not be satisfied by the SiO_X. This reduced hydrogen content is attributed to the assumption that the hydrogen is located at the grain boundaries. With increasing crystallite size, the amount of grain boundaries decreases, thus decreasing the hydrogen content. Another mechanism proposed for a reduced passivation quality of the layers at higher filament temperature is an increase in hydrogen radical density, which bombard and damage the wafer's surface and rupture Si—H and Si—O bonds at the SiO_X/c–Si interface, increasing the number of recombination centers. A thin interlayer of low-T_f, the passivation layer, is needed to allow enough hydrogen to get incorporated and assure a high passivation and a high-T_f layer, the conduction layer, is needed for a low contact resistance. It is also found that the FF of the cells is strongly influenced by the thickness of the passivation layer.[24]

After discussing different doping approaches and other means to tune the properties of nc-SiC:H, the following sections first revisit the influence of different deposition parameters on the optoelectrical properties of intentionally nitrogen-doped nc-SiC:H(n). The parameter series, which were previously studied

for HWCVD, will be re-evaluated and extended to include T_f, $d_{f\text{-}s}$, c_H, the total flow F_{total}, as well as a variation of the base pressure during deposition p_{base}, the temperature of the chamber heater T_{heater} and the nitrogen flow F_{N2}. In the second part, the influence of the layer thicknesses in the double-layer stack containing the passivating and the conducting layer will be analyzed and the influence on solar cell behavior will be evaluated.

3. Optoelectrical Properties of nc-SiC:H(n)

Figure 1 shows the conductivity and **Table 1** processes parameters of nc-SiC:H(n) for all series of samples investigated here. The conductivity can be increased by up to nine orders of magnitude, from 10^{-11} to 10^{-2} S cm^{-1}, by increasing T_f (Figure 1g) and c_H (Figure 1d). Up to four orders of magnitude increase can be achieved by reducing F_{total} (Figure 1f). For very low flow rates, the total layer thickness deposited during a fixed deposition time was too thin to ensure good conductivity.[13] It can be expected that the trend of increasing conductivity with decreasing flow rate, as seen for high flow rates, continues for low flow rates, if the layer thickness of the samples is increased. Other deposition parameters used in this study have a minor influence on the conductivity. For a decreased deposition pressure (Figure 1a) and increased heater temperature (Figure 1c), as well as increased N_2 doping gas flow rate (Figure 1f), only a minor increase in conductivity, within one order of magnitude, can be observed.
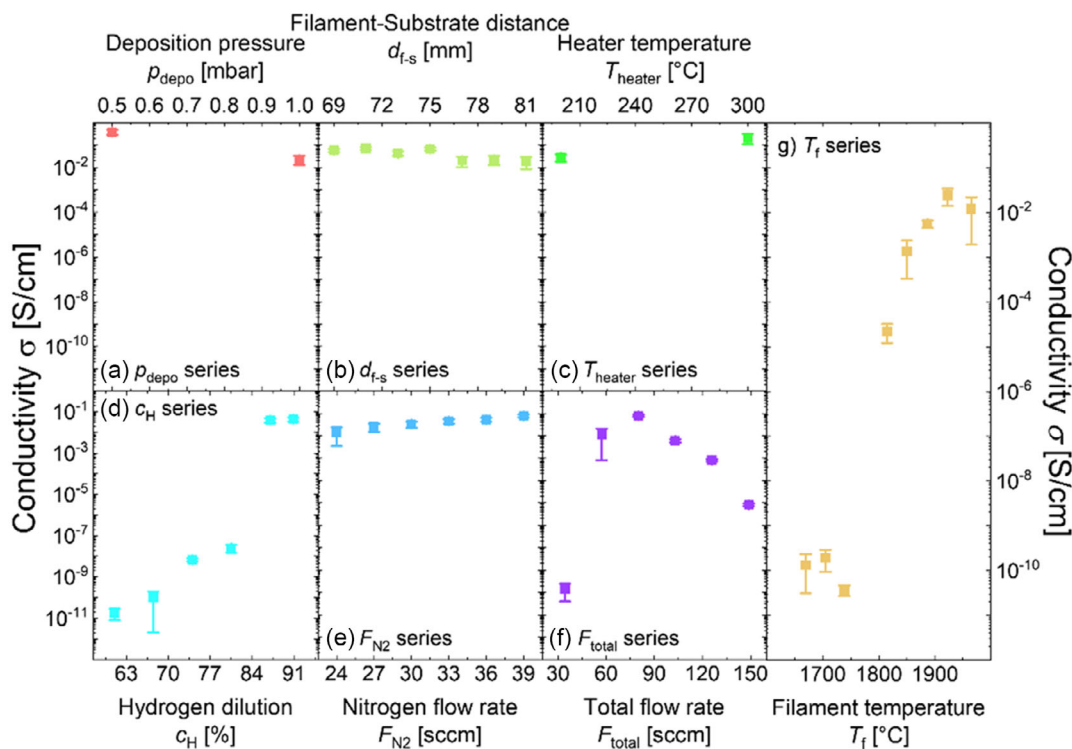

Figure 1. Electrical conductivity for nc-SiC:H(n) for varying a) deposition pressure, b) filament–substrate distance, c) chamber heater temperature, d) hydrogen dilution, e) nitrogen flow, f) total flow, and g) filament temperature. The filament temperature and the hydrogen diluted are the main levers to increase the conductivity, increasing it by nine orders of magnitude for high filament temperatures or high hydrogen dilution. Another strong increase in conductivity by four orders of magnitude can be achieved by reducing the total gas flow. The deposition pressure, filament–substrate distance, heater temperature, and doping gas flow only play a minor part in increasing the conductivity.

Table 1. Deposition parameter for the different series of nc-SiC:H(n) layers used in this work. The varied parameter is printed in bold.

Series	F_{MMS} [sccm]	F_{H2} [sccm]	F_{N2} [sccm]	F_{total} [sccm]	T_{heater} [°C]	p_{base} [mbar]	d_{f-s} [mm]	I_f [A]	T_f [°C]
p_{base} variation	7	70	25	77	250	**0.5–1.0**	71	49	1955 ± 63
T_f variation	9	94	30	103	250	0.75	79	**34–50**	**1670–1965**
d_{f-s} variation	9	94	30	103	250	0.75	**69–81**	49	1975 ± 13
T_{heater} variation	7	70	25	77	**200–300**	0.75	71	49	1993 ± 66
c_H variation	**7–30**	**70–47**	25	77	250	0.75	71	49	1989 ± 7
F_{N2} variation	9	94	**24–39**	103	250	0.75	79	50	1989 ± 5
F_{total} variation	3–13	31.3–135.5	10–43.3	**34.3–148.8**	250	0.75	79	46	1933 ± 4

The filament–substrate distance does not influence the conductivity (Figure 1b) in the investigated range. Since the increased doping gas flow, in the range studied here, only increases the conductivity to a minor extent, doping might not to be the driving force for the increase in electrical conductivity in nc-SiC:H(n) films. The increase in conductivity due to doping is most likely compensated by the decrease due to smaller crystallites.

The conductivity σ for different series is plotted versus the growth rate r in **Figure 2**. The general trend indicated that a reduction in the deposition rate is favorable for an increased dark conductivity. The only sample at a deposition rate of 2.5 nm min^{-1} has a higher conductivity as compared to other series and was deposited at a reduced heater temperature T_{heater}. For the lowest deposition rates in the total flow series, again the layer thickness is too thin to achieve a reasonable conductivity. It is expected that, if the layers are thicker, the conductivity would follow the general trend. For the nc-SiC:H(n), a low deposition rate and a minimum thickness to obtain the necessary conductivity are needed.

In **Figure 3**, the optical bandgap E_{04} is plotted against the conductivity. For an increased conductivity, a higher optical bandgap, indicating a higher transparency of the material, can be observed. So a highly conductive material with high transparency can be realized by depositions with a low growth rate.
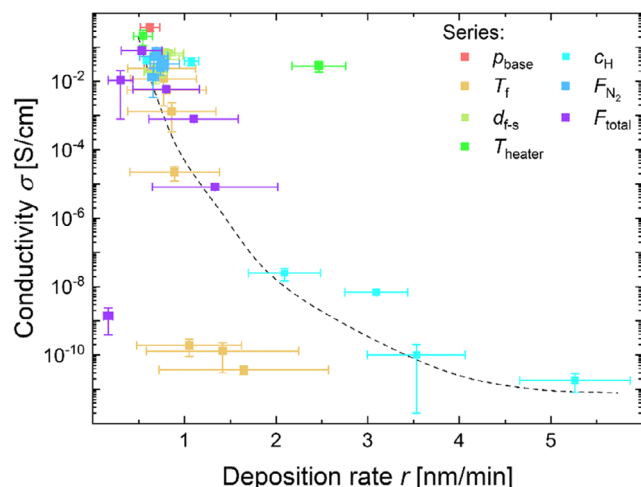
It is expected that the increase in conductivity originates from an increase in crystallite size;[13] thus, it is worth to take a closer look at the growth mechanisms. The two biggest influences on the conductivity, c_H and T_f, both increase the hydrogen radical density in the chamber.[26] The hydrogen radicals etch the weakly bonded atoms and increase the crystallite size. A reduced F_{total} reduces the number of molecules on the sample, which then do not hinder each other to reach their favorable bonding site, again increasing grain size. The same, even though to a smaller extend, might be true for the increased p_{depo}. The overall sample temperature is influenced by d_{f-s}, T_{heater}, and, to some extent, T_f. The increased temperature might enhance the mobility of molecules on the surface and can help find favorable bonding sites, leading to larger crystallites.

For larger crystallites, the nitrogen content increases in the samples and, at least for larger crystallites from higher T_f, the doping activation increases.[24] It is not known if this doping activation originates from the filament temperature itself or from the crystallite size. Nevertheless, from the F_{N2} series, it is found that an increased doping concentration studied in this work only makes minor contributions to a conductivity increase. For doping gas concentrations investigated in this case, this leads to the conclusion that the conductivity is, similar to the unintentionally doped case, mostly influenced by grain sizes and/or hydrogen passivation of the donors.[13] A higher doping concentration could be offset by a reduced crystallite size due to the introduction of dopants. If the conductivity is hindered by hydrogen passivation of the donors, it should increase if the hydrogen effuses from the sample.

The number of catalytic filaments used for the decomposition of precursor gases was not examined here. It can be expected that the number of filaments influences the sample temperature and the number of molecules on the sample. A higher number of filaments means more heat radiating from the filaments, heating the sample, and increasing the temperature. Also, more precursor gas molecules would be decomposed, leading to more molecules in the sample. The latter effect is similar to that of an increased total flow, which is a stronger effect than the sample temperature. For more filaments, the conductivity might, thus, decrease.

4. Behavior of nc-SiC:H(n) Layers in Solar Cells

It was found previously[24] that there is a direct trade-off in T_f between passivation quality and conductivity of the layers and,
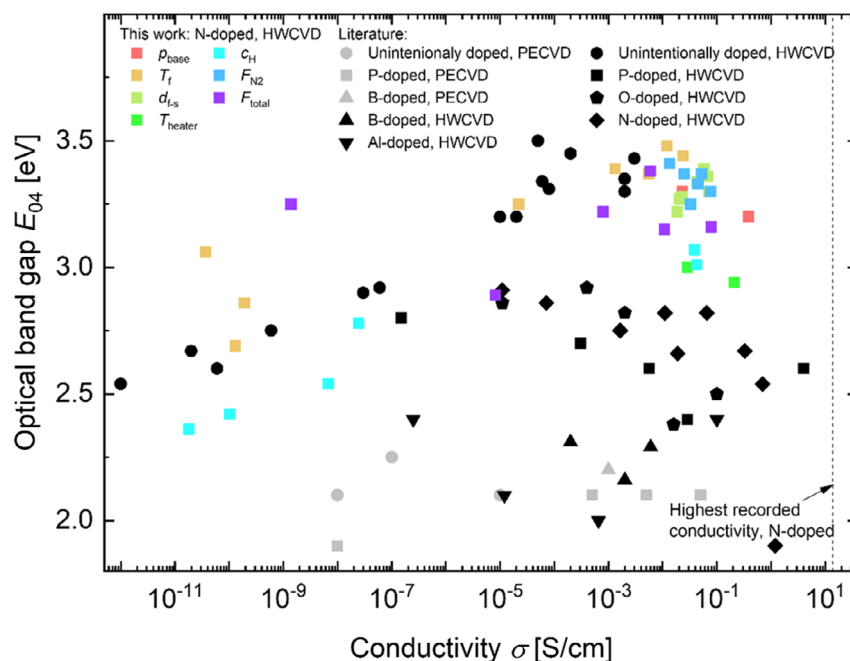

Figure 2. Conductivity of the different sample series compared to their film growth rate. A lower growth rate is highly favorable for a high conductivity.

Figure 3. Optical bandgap versus the electrical conductivity for various series of nc-SiC:H(n) layers investigated (colored points). Both a high E_{04} and σ are favorable layer properties. The black-gray points are extracted from the literature.[13,16,17,19,22]

thus, a layer stack consisting of a thinner passivating layer prepared at lower T_f and a thicker conducting layer prepared at higher T_f is proposed. The increased passivation for the low-T_f layer can be explained by the decreased crystallite size which leads to less hydrogen in the layers.[13] So large crystallites lead, on one hand, to a better conductivity and larger optical bandgap, but on the other hand to less hydrogen in the layer and, thus, a

worse passivation of dangling bonds of the crystalline silicon absorber. For that reason, in this part, the dependency of the solar cell parameters on each layer in the layer stack is systematically investigated.

Four different layer thicknesses are investigated, and the corresponding photovoltaic parameters are summarized in **Figure 4**. The efficiency η, implied open-circuit voltage iV_{OC}, and
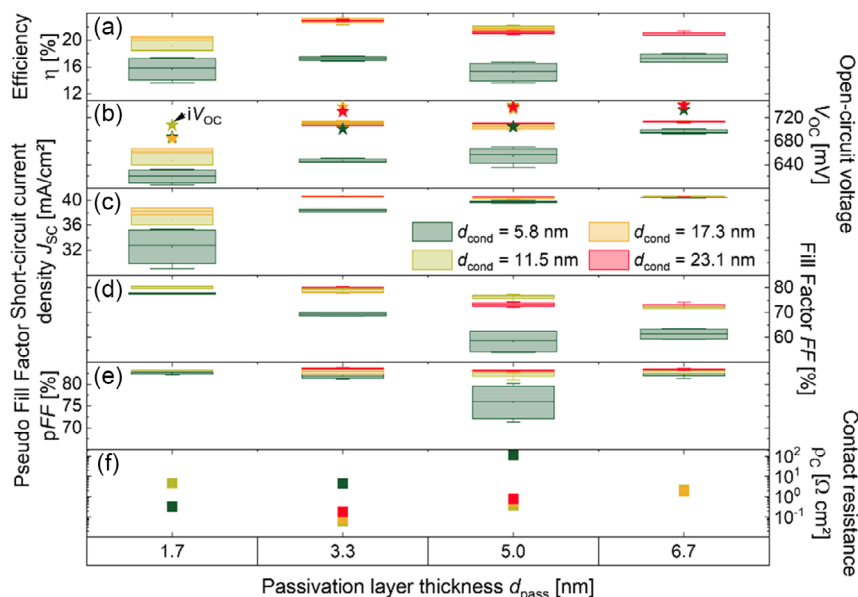

Figure 4. a) Efficiency, b) open-circuit voltage, c) short-circuit current density, d) fill factor, e) pseudo-fill factor, and f) contact resistance for different passivating and conducting layer thicknesses. The layer thicknesses are estimated for growth on glass substrates.
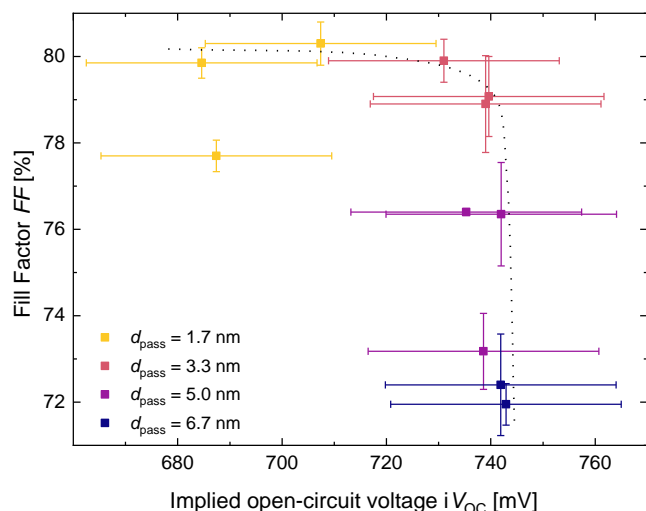
Figure 5. Fill factor versus iV_{OC} for different passivation and layer thicknesses. There is a direct trade-off between the FF and iV_{OC} with only a rather narrow regime for optimization. The dashed line is a guide to the eye.

open-circuit voltage V_{OC}, short-circuit current density J_{SC}, fill factor FF, pseudo-fill factor pFF, and contact resistance ρ_C are presented, depending on the passivating and conducting layer thicknesses, d_{pass} and d_{cond}, respectively. No strong influence of the conduction layer thickness on the cell parameters can be seen after a thickness of 11.5 nm is reached. For thicknesses below 11.5 nm, there might not be enough hydrogen in the layer stack to passivate the open Si-bonds at the crystalline silicon interface. Also, the thickness might be too thin for a good

conductivity, leading to extraction problems, as will be discussed later. These effects reduce the V_{OC}, as well as the FF and, to some extent, the J_{SC} of the solar cells. The maximum efficiency can be achieved with a conduction layer thickness above 5.8 nm and an intermediate passivation layer thickness. If the passivation layer is too thin, not enough hydrogen might be incorporated in the first few nanometers to fully satisfy the dangling bonds and hydrogen radical bombardment from the deposition of the conduction layer might damage the crystalline silicon interface. If the layer gets thicker, the iV_{OC}, indicating the quality of passivation, stays on a high level, but the FF start to reduce. As the pFF stays constant, the resistance of the layer stack might become problematic. This is underlined by the increase in ρ_C for increasing passivation layer thicknesses. ρ_C also increases for the thinnest conduction layer, indicating a conductivity problem. If the overall layer stack is too thin, also the J_{SC} is reduced, which could be explained by increased reflection, as will be discussed later.

The passivation layer should be sufficiently thick for a high iV_{OC} to incorporate enough hydrogen and protect the interface from undesirable hydrogen radical bombardment, in contrast, the FF decreases for thicker layers, so the FF is plotted against the iV_{OC} in **Figure 5** for different layer thicknesses. It is found that there is a direct trade-off between the FF and iV_{OC}, with only a narrow regime to optimize the passivation layer thickness before it either hinders charge carrier extraction or lacks passivation.

The reflection curves of the solar cells are shown in **Figure 6**a. The reflectance peak in the low wavelength regime is reduced and shifts to larger wavelength. The reflection between wavelength of 550 and 1000 nm is reduced as well. These two effects are also visible in the calculated reflection losses J_{refl} in Figure 6b, when the measured reflectance curve is multiplied by the
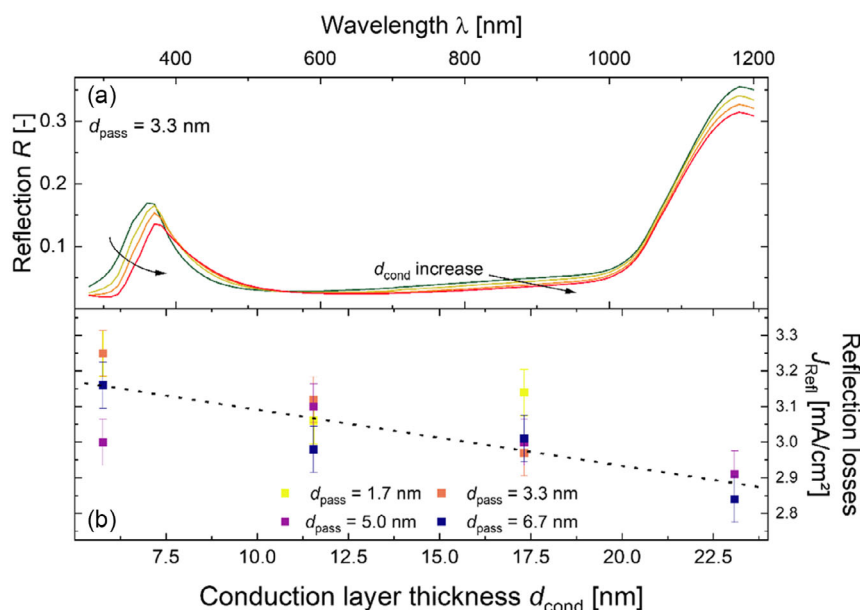

Figure 6. a) Reflection measurements and b) calculated reflection losses J_{refl} for a given passivation layer thickness with varying conduction layer thicknesses. It is found that, for thicker layers, the reflection maximum at low wavelength is reduced and shifted to higher wavelength. Between 550 and 1000 nm, the overall reflection is reduced. The reduced measured reflection for thicker conduction layers is also visible in a reduction in J_{refl}.
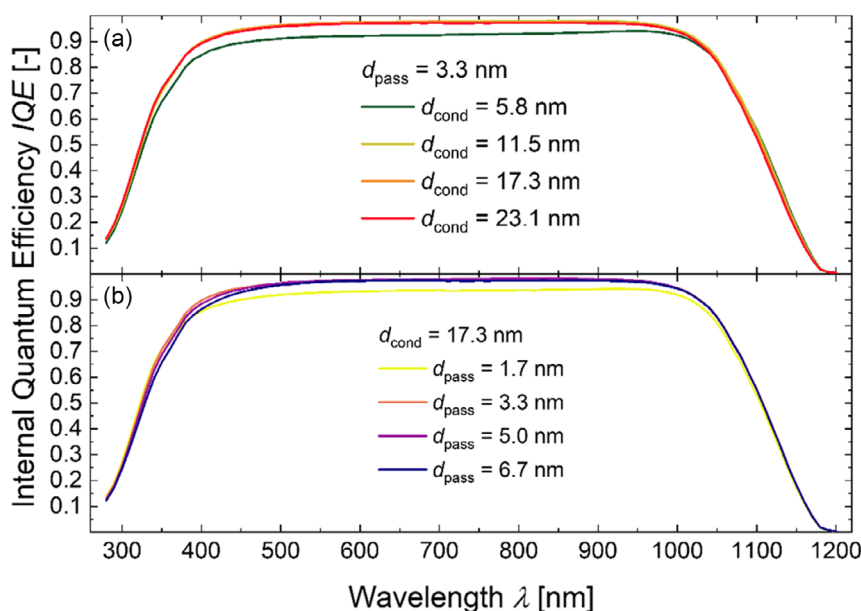
Figure 7. IQE curves for a) a fixed passivation layer thickness with varying conduction layer thicknesses and b) with a fixed conduction layer thickness and varying passivation layer thicknesses.

AM1.5G spectrum and integrated over the wavelength between 300 and 1200 nm. For thicker conduction layers, the overall reflection losses decrease. For only nc-SiC:H(n) layers, without any indium tin oxide (ITO) deposited on it, it is simulated that the lowest current losses are for thicknesses of 30 nm, as then the reflection loss is lowest, and the parasitic absorption is in an intermediate region. For thicker layers, the reflection losses should first decrease a little more, then start to increase. The parasitic absorption losses increase for thicker layers.[25] For this work, the layer thicknesses are all below 30 nm, so the observed trend is as expected. Also, no direct translation from reduced J_{refl} to increased J_{SC} could be found. This phenomenon is still under investigation. It can be speculated that the light, which is not reflected, is instead parasitically absorbed in, for example, the ITO.

Lastly, the internal quantum efficiencies (IQE) for a given passivation layer thickness and conduction layer thickness are given in **Figure 7**a,b, respectively. For both, very thin passivation or conduction layer thicknesses, the IQE is overall reduced. For thin conduction layer thicknesses, two effects might come into play. The collection of charge carriers could be hindered, as the FF in Figure 4d is also reduced, due to a higher layer resistance from a reduced layer thickness. Also, a reduced iV_{OC} can be found in Figure 4b, indicating a reduced passivation, which might lead to the reduction in IQE. For very thin passivation layers, the FF is not reduced but the iV_{OC} even more so. The IQE has a similar reduced shape between 400 and 1000 nm. Thus, the reduction in IQE might be due to a poor quality of passivation. Since the IQE also relies on the diffusion length of the charge carriers in the sample, the diffusion length might be reduced due to recombination, leading to the lower IQE.[27]

5. Summary and Outlook

In this work, it is shown that the dark conductivity of nitrogen-doped nc-SiC:H(n) can be tuned over a wide range within 10 orders of magnitude between 10^{-11} and 10^{-1} S cm^{-1}. Herein, the main parameters to control the conductivity variations are filament temperature and hydrogen dilution resulting in a variation over nine orders of magnitude in σ, followed by the total flow rate (five orders of magnitude variations). We found that the other deposition parameters, such as heater temperature, filament–substrate distance, deposition pressure, and nitrogen flow only have a minor influence on the conductivity (below an order of magnitude) over the investigated ranges. The remarkable increase in conductivity can be related to an increased crystallite grain size and/or reduced hydrogen passivation of the donor centers. The increase in conductivity is also accompanied with an increase in the optical bandgap, which increases from around 2.4 eV for low conductivities to 3.4 eV for high-conductivity materials.

The large crystallite size needed for high conductivities and large optical bandgaps can only be achieved with a low deposition rate below 1 nm min^{-1}. For higher deposition rates, a drastic decrease in conductivity is observed. The influence in crystallite size can be broken down into three processes during layer growth. A higher sample temperature, achieved by a reduced $d_{f\text{-}s}$ or increased T_f and T_{heater}, can lead to an increased mobility of the molecules on the sample, making it easier for them to find an energetically favorable spot before they settle, leading to larger crystallites. A hindrance to finding a favorable position is an increased number of molecules on the sample, since they could interfere with one another. This might lead to more active crystallite growth sides in the beginning, more crystallites growing

and hindering each other, leading to a reduced crystallite size in the end. The number of molecules could be reduced by a reduction in F_{total} and p_{depo}. The most prominent influence on the growth of the material is the hydrogen radical density. The radicals etch weakly bonded molecules, that is, molecules on unfavorable sites, leading to larger crystallites. The hydrogen radical density is influenced by T_f and c_H. Lastly, variations in F_{N2} do not show a strong influence on the conductivity, suggesting that there is a trade-off between increased doping concentration and decreased crystallite size due to increased number of impurities.

The implementation of the double-layer stack of the passivating and conducting layer into the solar cell is further investigated and dependencies of cell parameter on the different layer thicknesses are studied. For the case of passivation layer, a thicker layer increases the iV_{OC} but decreases the FF. Due to the low conductivity of the layer, the solar cell could face extraction problems when the thickness of the layer is increased above 3.3 nm. A direct trade-off between the iV_{OC} and the FF is observed, which is one of the limiting factors to the overall cell performance. For the case of the conductive layer, after a thickness of around 11.5 nm is reached, no strong dependency of the layer thickness on photovoltaic performance is found. It is postulated that this thickness is needed to incorporate enough hydrogen into the thin passivation layer for a suitable interface passivation. A reduction in reflection losses is found for increased layer thicknesses, but no increase in J_{SC} is observed, which could be due to an increased parasitic absorption for thicker layers.

The two main challenges which need to be overcome to keep the TPC competitive with other novel approaches are the iV_{OC}–FF trade-off for the passivation layer thickness, as discussed in this work, and the reduction in V_{OC} after sputtering, as discussed elsewhere.[8]

6. Experimental Section

The samples for conductivity measurements and optical bandgap determination in the third section were deposited on glass from Corning-type Eagle. The nitrogen-doped nc-SiC:H(n) layers were deposited using a HWCVD system from MRG systems with three curled Rhenium filaments with a diameter of 0.5 mm. The process parameter for each sample series can be found in Table 1, where the varied deposition parameters are in bold letters. The deposition time was held constant at 30 min for all samples. The temperature was measured with a Raytek Marathon series differential pyrometer with a given error of $\pm 20\,°C$. The thickness d was measured with a Dektak 6M Stylus Profiler profilometer on glass substrates. The deposition rate was determined by dividing the measured thickness by the deposition time, as given in Table 1. The conductivity was measured by an in-house build setup, which contacts the sample through two evaporated coplanar silver contacts. The transmission (T) and reflection (R) were measured with a Perkin Elmer Lambda 950 UV/vis spectrometer. From these data, the absorption coefficient (α) was calculated by using the following equation

$$\frac{T}{1-R} = \exp(-\alpha * d) \tag{1}$$

The optical bandgap (E_{04}) was the photon energy at which $\alpha = 10^4\,cm^{-1}$.

The solar cells in section four were fabricated on double-side textured, quartered M2-sized n-type wafers with a thickness of 135 μm, a resistivity
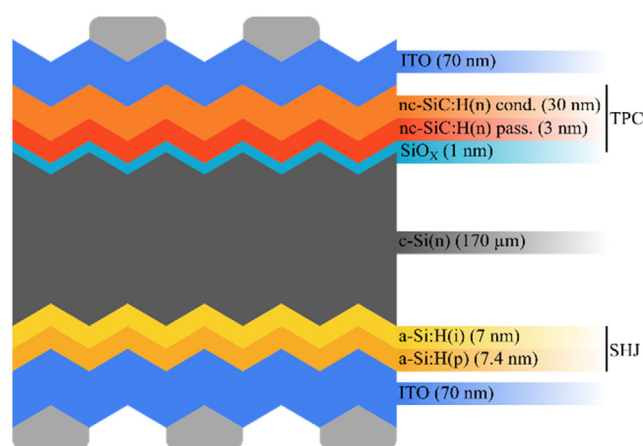

Figure 8. Cross-section of the used solar cell structure. The transparent passivating contact acts as the front contact, while a standard i/p a-Si:H SHJ contact acts as rear junction.

of $1\,\Omega\,cm$ and $<100>$ crystalline orientation supplied by LONGi. The wafers were cleaned using DIO_3 treatment. Afterward, they were dipped in 1% hydrofluoric acid and a wet-chemical oxide was grown by submerging the wafers in Piranha solution with a H_2O_2:H_2SO_4 mixture of 2:1 for 10 min. The nc-SiC:H(n) was deposited in the same HWCVD system as previously described. The passivation and conduction layer were deposited without stopping the process by ramping up the filament current (and, thus, its temperature) with a ramping rate of $2\,A\,s^{-1}$. All samples used a filament–substrate distance d_{f-s} of 71 mm, a MMS flow of 7 sccm, a hydrogen (H_2) flow of 70 sccm, and a nitrogen (N_2) flow of 25 sccm at a heater temperature T_{heater} of $250\,°C$ and a pressure during deposition p_{base} of 0.75 mbar. The passivating layer was deposited at a filament temperature T_f of $1660\,°C$ and the conducting layer was deposited at a T_f of $1930\,°C$. The layer thicknesses were calculated from deposition rates measured on glass. The intrinsic and p-type amorphous silicon layers on the rear side were deposited using the industrial PECVD tool AK1000 Inline from Meyer Burger, forming the pn-junction at the rear side of the cell. Between the HWCVD and PECVD deposition, another dip in 1% HF solution was performed to remove the previously grown oxide on the rear side. The ITO was sputtered, and the silver contacts were screen-printed by a MT-650TVC screen printer from Micro-tec and were annealed in an oven for 40 min at $170\,°C$. A cross-section of the resulting solar cell can be found in **Figure 8**. The solar cells were then cured on a hot plate for 20 min at $230\,°C$ and additionally light soaked for 90 s at $210\,°C$. After the PECVD deposition, the implied open-circuit voltage iV_{OC} at one sun was measured by a Sinton WTC-120 lifetime tester. All solar cell characterization was done with the LOANA tool from pv-tools with a Sinus 220 LED light source from Wavelabs.

Conflict of Interest

The authors declare no conflict of interest.

Data Availability Statement

The data that support the findings of this study are available from the corresponding author upon reasonable request.

[1] T. G. Allen, J. Bullock, X. Yang, A. Javey, S. De Wolf, *Nat. Energy* **2019**, *4*, 914.

[2] C. Ballif, F.-J. Haug, M. Boccard, P. J. Verlinden, G. Hahn, *Nat. Rev. Mater.* **2022**, *7*, 597.

[3] Z. C. Holman, A. Descoeudres, L. Barraud, F. Z. Fernandez, J. P. Seif, S. De Wolf, C. Ballif, *IEEE J. Photovoltaics* **2012**, *2*, 7.

[4] J. Ibarra Michel, J. Dréon, M. Boccard, J. Bullock, B. Macco, *Prog. Photovoltaics Res. Appl.* **2022**, 1.

[5] M. Boccard, Z. C. Holman, *J. Appl. Phys.* **2015**, *118*, 065704.

[6] D. Zhang, D. Deligiannis, G. Papakonstantinou, R. A. C. M. M. Van Swaaij, M. Zeman, *IEEE J. Photovoltaics* **2014**, *4*, 1326.

[7] S. Miyajima, in *2014 21st Inter. Workshop on Active-Matrix Flatpanel Displays and Devices (AM-FPD)*, IEEE, Kyoto, Japan **2014**, p. 65.

[8] M. Köhler, M. Pomaska, P. Procel, R. Santbergen, A. Zamchiy, B. Macco, A. Lambertz, W. Duan, P. Cao, B. Klingebiel, S. Li, A. Eberst, M. Luysberg, K. Qiu, O. Isabella, F. Finger, T. Kirchartz, U. Rau, K. Ding, *Nat. Energy* **2021**, *6*, 529.

[9] Z. Xu, K. Tao, S. Jiang, R. Jia, W. Li, Y. Zhou, Z. Jin, X. Liu, *Sol. Energy Mater. Sol. Cells* **2020**, *206*, 110329.

[10] Y. Tawada, H. Okamoto, Y. Hamakawa, *Appl. Phys. Lett.* **1981**, *39*, 237.

[11] Y. Huang, A. Dasgupta, A. Gordijn, F. Finger, R. Carius, *Appl. Phys. Lett.* **2007**, *90*, 203502.

[12] T. Chen, Y. Huang, A. Dasgupta, M. Luysberg, L. Houben, D. Yang, R. Carius, F. Finger, *Sol. Energy Mater. Sol. Cells* **2012**, *98*, 370.

[13] M. B. Pomaska, *Microcrystalline Silicon Carbide for Silicon Heterojunction Solar Cells*, Forschungszentrum Jülich, Jülich, Germany **2017**.

[14] S. Miyajima, J. Irikawa, A. Yamada, M. Konagai, *Appl. Phys. Lett.* **2010**, *2*, 97.

[15] K. Shimizu, A. E. Omondi, J. Irikawa, S. Miyajima, M. Konagai, in *2014 IEEE 40th Photovoltaic Specialist Conf. (PVSC)*, IEEE, Denver, CO, USA **2014**, p. 1253.

[16] F. Demichelis, C. F. Pirri, E. Tresso, *J. Appl. Phys.* **1992**, *72*, 1327.

[17] S. Miyajima, A. Yamada, M. Konagai, *Jpn. J. Appl. Phys.* **2007**, *46*, 1415.

[18] S. Kerdiles, A. Berthelot, F. Gourbilleau, R. Rizk, *Appl. Phys. Lett.* **2000**, *76*, 2373.

[19] T. Chen, A. Schmalen, J. Wolff, D. Yang, R. Carius, F. Finger, *Phys. Status Solidi C* **2010**, *7*, 754.

[20] H. Matsumura, H. Umemoto, K. K. Gleason, R. E. Schropp, *Catalytic Chemical Vapor Deposition: Technology and Applications of Cat-CVD*, John Wiley & Sons, Hoboken, New Jearsey, USA **2019**.

[21] F. Köhler, *Zur Mikrostruktur siliziumbasierter Dünnschichten für die Photovoltaik*, Forschunsgzentrum Jülich, Jülich, Germany **2012**.

[22] A. Pawbake, A. Mayabadi, R. Waykar, R. Kulkarni, A. Jadhavar, V. Waman, J. Parmar, S. Bhattacharyya, Y. R. Ma, R. Devan, H. Pathan, S. Jadkar, *Mater. Res. Bull.* **2016**, *76*, 205.

[23] J. Y. Seto, *J. Appl. Phys.* **1975**, *46*, 5247.

[24] M. Köhler, *Transparent Passivating Contact for Crystalline Silicon Solar Cells*, Forschungszentrum Jülich, Jülich, Germany **2020**.

[25] M. Pomaska, M. Köhler, P. P. Moya, A. Zamchiy, A. Singh, D. Y. Kim, O. Isabella, M. Zeman, S. Li, K. Qiu, A. Eberst, V. Smirnov, F. Finger, U. Rau, K. Ding, *Prog. Photovoltaics Res. Appl.* **2020**, *28*, 321.

[26] H. Umemoto, K. Ohara, D. Morita, Y. Nozaki, A. Masuda, H. Matsumura, *J. Appl. Phys.* **2002**, *91*, 1650.

[27] B. Fischer, *Loss Analysis of Crystalline Silicon Solar Cells using Photoconductance and Quantum Efficiency Measurements*, Cuvillier Verlag, Göttingen, Germany **2003**.